

MeTA: Multi-source Test Time Adaptation

Sk Miraj Ahmed^{1,*}, Fahim Faisal Niloy^{1,*}, Dripta S. Raychaudhuri^{2,†}, Samet Oymak³, Amit K. Roy-Chowdhury¹

¹University of California, Riverside ²AWS AI Labs ³University of Michigan, Ann Arbor

{fnilo001@, sahme047@, drayc001@, amitrc@ece.{ucr.edu, oymak@umich.edu}

Abstract

Test time adaptation is the process of adapting, in an unsupervised manner, a pre-trained source model to each incoming batch of the test data (i.e., without requiring a substantial portion of the test data to be available, as in traditional domain adaptation) and without access to the source data. Since it works with each batch of test data, it is well-suited for dynamic environments where decisions need to be made as the data is streaming in. Current test time adaptation methods are primarily focused on a single source model. We propose the first completely unsupervised Multi-source Test Time Adaptation (MeTA) framework that handles multiple source models and optimally combines them to adapt to the test data. MeTA has two distinguishing features. First, it efficiently obtains the optimal *combination* weights to combine the source models to adapt to the test data distribution. Second, it identifies which of the source model parameters to update so that only the model which is most correlated to the target data is adapted, leaving the less correlated ones untouched; this mitigates the issue of “forgetting” the source model parameters by focusing only on the source model that exhibits the strongest correlation with the test batch distribution. Experiments on diverse datasets demonstrate that the combination of multiple source models does at least as well as the best source (with hindsight knowledge), and performance does not degrade as the test data distribution changes over time (robust to forgetting).

Introduction

Deep neural networks have shown impressive performance on test inputs that closely resemble the training distribution. However, their performance degrades significantly when they encounter test inputs from a different data distribution. Unsupervised domain adaptation (UDA) techniques (Tzeng et al. 2017; Tsai et al. 2018) aim to mitigate this performance drop in the face of distribution shift but, require a large number of samples from the test distribution which is often impractical. Test-time adaptation (TTA) (Wang et al. 2020) has emerged as a promising approach that enables models to adapt to new domains at test time, in an online fashion, without requiring any additional training data. TTA is typically achieved by updating the source model parameters through a few rounds

*Equal contribution.

†Currently at AWS AI Labs. Work done while the author was at UCR.

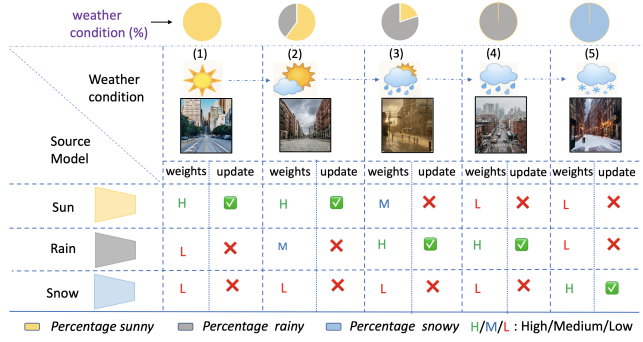


Figure 1: Problem setup. Consider that we have several source models that were trained using data from different weather conditions. During the deployment of these models, they may encounter varying weather conditions over time that could be a combination of multiple conditions in varying proportions (represented by the pie charts on top). Our goal is to infer on the test data using the ensemble of models by automatically figuring out proper combination weights and adapting the models on the fly.

of optimization using an unsupervised objective that incorporates the new test sample from the target distribution, where the target distribution can either be stationary (Wang et al. 2020) or dynamically changing (Wang et al. 2022b).

Current TTA methods rely on a single source model during adaptation. However, situations may arise wherein the user has access to a diverse set of pre-trained models across distinct source domains. In those scenarios, it is both reasonable and effective to employ and adapt the entire available array of source models during testing, thereby enhancing performance beyond the scope of single source model adaptation. Additionally, the utilization of multi-source TTA presents the flexibility to seamlessly add or remove models even after deployment, according to the user’s preferences and demands of the task at hand.

Combining models from various source domains can offer a more holistic perspective of the target domain. This is particularly true when different source domains possess distinct characteristics relevant to the task at hand. Take for instance a scenario where a recognition model, initially trained on clear weather conditions, faces data from mixed weather scenarios, like sunshine interspersed with rain (refer to Figure 1). In

Table 1: **Comparison of our setting to the existing adaptation settings.** Our proposed setting meets all the criteria that are expected in a comprehensive adaptation framework.

Setting	Source Free	Adaptation On the Fly	Dynamic Target	Multi Source
UDA	✗	✗	✗	✓
Source-free UDA	✓	✗	✗	✓
TTA	✓	✓	✓	✗
MeTA	✓	✓	✓	✓

such cases, employing multiple models—specifically those trained on clear weather and rain—with appropriate weighting can potentially reduce the test error as opposed to relying on a single source model. In this context, the models for clear weather and rain would be assigned higher weights, while other models representing different weather conditions would receive relatively lesser weightage.

The main challenge of developing such a multi-source TTA method is to *learn appropriate combination weights to optimally combine the source model ensemble during the test phase as data is streaming in, such that it results in a test accuracy equal or higher than that of the best source model*. To solve this, we propose the first fully unsupervised Multi-source Test Time Adaptation (MeTA) framework that handles multiple source models and optimally combines them to adapt to the test data. While the multi-source setting has been addressed in UDA (Ahmed et al. 2021), the problem remains open in the TTA scenario.

The efficacy of using multiple source models also extends to preventing the *catastrophic forgetting* associated with TTA methods in the dynamic setting (Wang et al. 2022b). Consider again the scenario of multiple source models, each trained on a different weather condition. During inference, only the parameters of the models most closely related to the weather encountered during test time will get updates, and the unrelated ones will be left untouched. This ensures that the model parameters do not drift too far from the initial state, since only those related to the test data are being updated. This mechanism mitigates forgetting when the test data distribution varies over a long time scale, as is likely to happen in most realistic conditions. Even if an entirely unrelated distribution appears during testing and there is no one source model to handle it, the presence of multiple sources can significantly reduce the rate at which the forgetting occurs. This is again because only the most closely related models (clear and rainy weather in the example above) are updated, while others (e.g., snow) are left untouched.

Main Contributions. Our proposed framework, MeTA, makes the following contributions.

- To the best of our knowledge, this is the first work to identify the problem of Multi-source test Time Adaptation (MeTA) in a completely unsupervised setting and develop an effective solution. Our approach has the ability to merge the source models using appropriate combination weights during test time, enabling it to perform just as well as the best-performing source or even surpass it.
- Our framework is both intuitive and easy to implement, yet it not only achieves performance on par with the best-

performing source, but it also effectively mitigates catastrophic forgetting when faced with long-term, fluctuating test distributions. Additionally, this algorithm has the capability to extend any current single source test time adaptation methods to the multi-source scenario, thereby increasing its versatility and simplicity of application.

- We provide theoretical insights on MeTA, illustrating how it addresses domain shift by optimally combining source models and prioritizing updates to the model least prone to forgetting.
- To demonstrate the real-world advantages of our methodology, we perform experiments on a diverse range of benchmark datasets.

Related Works

Unsupervised Domain Adaptation. UDA methods have been applied to many machine learning tasks, including image classification (Tzeng et al. 2017), semantic segmentation (Tsai et al. 2018), object detection (Hsu et al. 2020) and reinforcement learning (Raychaudhuri et al. 2021), in an effort to address the data distribution shift. Most approaches try to align the source and target data distributions, using techniques such as maximum mean discrepancy (Long et al. 2015), adversarial learning (Ganin et al. 2016; Tzeng et al. 2017; Raychaudhuri et al. 2021) and image translation (Hoffman et al. 2018; Tran et al. 2019).

Recently, there has been a growing interest in adaptation using only a pre-trained source model due to privacy and memory storage concerns related to the source data (Yang et al. 2021; Kundu et al. 2020; Wang et al. 2022a; Yang et al. 2020; Li et al. 2020; Ding et al. 2022; Chen et al. 2022). These approaches include techniques such as information maximization (Liang, Hu, and Feng 2020; Ahmed et al. 2021, 2022), pseudo labeling (Yeh et al. 2021; Kumar et al. 2023), and self-supervision (Xia, Zhao, and Ding 2021).

Test Time Adaptation. UDA methods typically require a substantial volume of target domain data for model adaptation, which is performed offline, prior to deployment. On the other hand, Test Time Adaptation (TTA) adjusts a model post-deployment, during inference or testing. One of the early works (Li et al. 2016) use test-batch statistics for batch normalization adaptation. TENT (Wang et al. 2020) updates a pre-trained source model by minimizing entropy and updating batch-norm parameters. DUA (Mirza et al. 2022) updates batch-norm stats with incoming test batches. TTA methods have also been applied to segmentation problems (Valanarasu et al. 2022; Shin et al. 2022; Liu, Zhang, and Wang 2021; Hu et al. 2021). When these TTA methods are used to adapt to changing target distribution, they usually suffer from ‘forgetting’ and ‘error accumulation’ (Wang et al. 2022b). In order to solve this, CoTTA (Wang et al. 2022b) restores source knowledge stochastically to avoid drifting of source knowledge. EATA (Niu et al. 2022) adds a regularization loss to preserve important weights for less forgetting. Compared to these methods, the proposed multi-source TTA approach has an inherent capability to mitigate forgetting.

Multi-Source Domain Adaptation (MSDA). Both UDA and source-free UDA have been extended to multi-source setting

by incorporating knowledge from multiple source models (Ahmed et al. 2021; Zhao et al. 2020). Notable techniques include discrepancy-based MSDA (Guo, Shah, and Barzilay 2018), higher-order moments (Peng et al. 2019), adversarial methods (Xu et al. 2018), and Wasserstein distance-based methods (Li, Carlson et al. 2018). However, these methods are specifically tailored to UDA scenarios, where the whole target data is assumed to be available during adaptation. Using multiple source models is still unexplored in the case of TTA. In a recent study by (Ye, Xie, and Ng 2023), the problem of multi-source TTA is addressed, but their method relies on user feedback, necessitating human intervention. In contrast, we approach this issue in a standard setting, akin to (Wang et al. 2020), where the process is entirely unsupervised, without requiring any human input.

Another related field is Domain Generalization (DG) (Dubey et al. 2021; Xiao et al. 2022), which refers to training a single model on a combined set of data from different target domains. Hence, DG requires data from all distinct domains to be available altogether during training, which may not be always feasible. In our problem, inspired by MSDA, users are only provided with pre-trained source models.

MeTA Framework

Problem Setting

In this problem setting, we propose to combine multiple pre-trained models during test time through the application of suitable combination weights, determined based on a limited number of test samples. Specifically, we will focus on the classification task that involves K categories. Consider the scenario where we have a collection of N source models, denoted as $\{f_S^j\}_{j=1}^N$, that we aim to deploy during test time. In this situation, we assume that a sequence of test data $\{x_i^{(1)}\}_{i=1}^B \rightarrow \{x_i^{(2)}\}_{i=1}^B \rightarrow \dots \rightarrow \{x_i^{(t)}\}_{i=1}^B \rightarrow \dots$ are coming batch by batch in an online fashion, where t is the index of time-stamp and B is the number of samples in the test batch. We also denote the test distribution at time-stamp t as $\mathcal{D}_T^{(t)}$, which implies $\{x_i^{(t)}\}_{i=1}^B \sim \mathcal{D}_T^{(t)}$. Motivated by (Ahmed et al. 2021), we model the test distribution in each time-stamp t as a linear combination of source distributions where the combination weights are denoted by $\{w_j^{(t)}\}_{j=1}^N$. Thus, our inference model on test batch t can be written as $f_T^{(t)} = \sum_{j=1}^N w_j^{(t)} f_S^{j(t)}$ where $f_S^{j(t)}$ is the adapted j -th source in time stamp t . Based on this setup our objective is twofold:

1. We want to determine the optimal combination weights $\{w_j^{(t)}\}_{j=1}^N$ for the current test batch such that the test error for the optimal inference model is lesser than or equal to the test error of best source model. Mathematically we can write this as follows:

$$\epsilon_{test}^{(t)}(f_T^{(t)}) \leq \min_{1 \leq j \leq N} \epsilon_{test}^{(t)}(f_S^j), \quad (1)$$

where $\epsilon_{test}^{(t)}(\cdot)$ evaluates the test error on t -th batch.

2. We also aim for the model to maintain consistent performance on source domains, as it progressively adapts to the changing test conditions. This is necessary to ensure that the model hasn't catastrophically forgotten the

original training distribution of the source domain and maintains its original performance if the source data is re-encountered in the future. We would ideally want to have:

$$\epsilon_{src}(f_S^{j(t)}) \approx \epsilon_{src}(f_S^j) \quad \forall j, t, \quad (2)$$

where, $\epsilon_{src}(f_S^j)$ denote the test error of j -th source on its corresponding test data when using the original source model f_S^j , whereas $\epsilon_{src}(f_S^{j(t)})$ represents the test error on the same test data using the j -th source model adapted up to time step t , denoted as $f_S^{j(t)}$.

Overall Framework

Our framework undertakes two operations on each test batch. First, we learn the combination weights for the current batch at time step t by freezing the model parameters. Then, we update the model corresponding to the largest weight with existing state-of-the-art TTA methods, which allows us to fine-tune the model and improve its performance. This implies that the model parameters of source j might get updated up to p times at time-step t , where $0 \leq p \leq (t-1)$.

In other words, the states of the source models evolve over time depending on the characteristics of the test batches up to the previous time step. To formalize this concept, we define the state of the source model j at time-step t as $f_S^{j(t)}$. In the next section, we will provide a detailed explanation of both aspects of our framework: (i) learning the combination weights, and (ii) updating the model parameters. By doing so, we aim to provide a comprehensive understanding of how our approach works in practice.

Learning the combination weights

For an unlabeled target sample $x_i^{(t)}$ that arrives at time-stamp t , we denote its pseudo-label, as predicted by source j , as $\hat{y}_{ij}^{(t)} = f_S^{j(t)}(x_i^{(t)})$, where $f_S^{j(t)}$ is the state of source j at time-stamp t . Now we linearly combine these pseudo-labels by source combination weights $\mathbf{w} = [w_1 \ w_2 \ \dots \ w_N]^\top \in \mathbb{R}^N$ to get weighted pseudo-label $\hat{y}_i^{(t)} = \sum_{j=1}^N w_j \hat{y}_{ij}^{(t)}$. Using these weighted pseudo-labels for all the samples in the t -th batch we calculate the expected Shannon entropy as,

$$\mathcal{L}_w^{(t)}(\mathbf{w}) = -\mathbb{E}_{\mathcal{D}_T^{(t)}} \sum_{c=1}^K \hat{y}_{ic}^{(t)} \log(\hat{y}_{ic}^{(t)}) \quad (3)$$

Based on this loss we solve the following optimization:

$$\begin{aligned} & \underset{\mathbf{w}}{\text{minimize}} \quad \mathcal{L}_w^{(t)}(\mathbf{w}) \\ & \text{subject to} \quad w_j \geq 0, \forall j \in \{1, 2, \dots, N\}, \\ & \quad \sum_{j=1}^n w_j = 1 \end{aligned} \quad (4)$$

Suppose we get $\mathbf{w}^{*(t)}$ to be the optimal combination weight vector by performing the optimization in (4). In such case, the optimal inference model for test batch t can be expressed as follows:

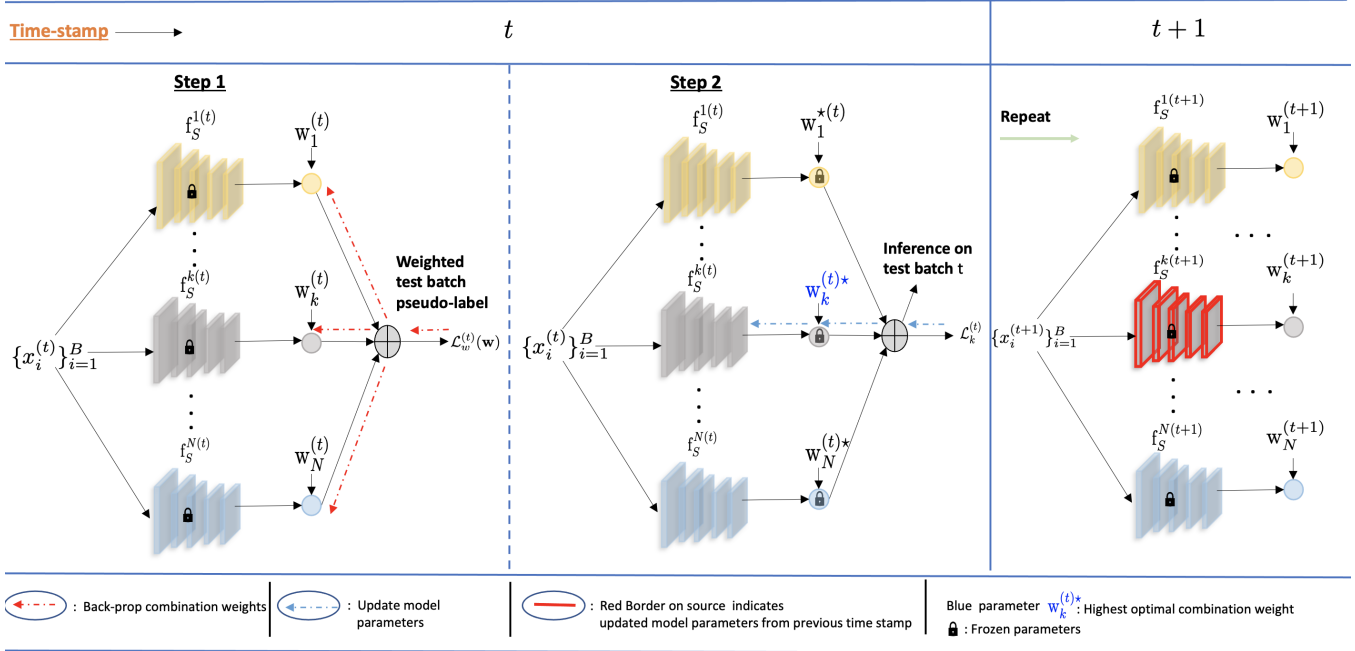


Figure 2: **Overall Framework.** During test time, we aim to adapt multiple source models in a manner such that it optimally blends the sources with suitable weights based on the current test distribution. Additionally, we update the BN parameters of only one model that exhibits the strongest correlation with the test distribution to use it for the inference task on the next test batch.

$$f_T^{(t)} = \sum_{j=1}^N w_j^{*(t)} f_S^{j(t)} \quad (5)$$

Thus, by learning w in this step, we satisfy Eqn. (1).

Model parameter update. After obtaining $w^{*(t)}$, next we select the most relevant source model k given by $k = \arg \max_{1 \leq j \leq N} w_j^{*(t)}$. This indicates that the distribution of the current test batch is most correlated with the source model k . We then adapt model k to the test batch t using state-of-the-art single source TTA methods. Specifically, we employ three distinct adaptation approaches: (i) TENT (Wang et al. 2020), (ii) CoTTA (Wang et al. 2022b), and (iii) EaTA (Niu et al. 2022). For a more in-depth discussion of these adaptation methods, please consult the supplementary material.

Optimization strategy for (4). Solving the optimization problem in Eq. 4 is a prerequisite for inferring the current test batch. As inference speed is critical for test-time adaptation, it is desirable to learn the weights quickly. To achieve this, we design two strategies: (i) selecting an appropriate initialization for w , and (ii) determining an optimal learning rate. **(i) Good initialization:** Pre-trained models contain information about expected batch mean and variance in their Batch Norm (BN) layers based on the data they were trained on. To leverage this information, we extract these stored values from each source model prior to adaptation. Specifically, we denote the expected batch mean and standard deviation for the l -th layer of the j -th source model as μ_l^j and σ_l^j , respectively.

During testing on the current batch t , we pass the data through each model and extract its mean and standard devi-

ation from each BN layer. We denote these values as $\mu_l^{T(t)}$ and $\sigma_l^{T(t)}$, respectively. One useful metric for evaluating the degree of alignment between the test data and each source is the distance between their respective batch statistics. A smaller distance implies a stronger correlation between the test data and the corresponding source. Assuming that the batch-mean statistic per node of the BN layers to be a univariate Gaussian, we calculate the distance (KL divergence) between the j -th source (approximated as $\mathcal{N}(\mu_l^j, (\sigma_l^j)^2)$) and the t -th test batch (approximated as $\mathcal{N}(\mu_l^{T(t)}, (\sigma_l^{T(t)})^2)$) as follows:

$$\theta_j^t = \sum_l \mathcal{D}_{KL} \left[\mathcal{N} \left(\mu_l^{T(t)}, (\sigma_l^{T(t)})^2 \right), \mathcal{N} \left(\mu_l^j, (\sigma_l^j)^2 \right) \right] = \sum_{l=1}^{n_j} \sum_{m=1}^{d_l^t} \log \left(\frac{\sigma_{lm}^j}{\sigma_{lm}^{T(t)}} \right) + \frac{(\sigma_{lm}^{T(t)})^2 + (\mu_{lm}^j - \mu_{lm}^{T(t)})^2}{2 (\sigma_{lm}^j)^2} - \frac{1}{2}$$

where subscript lm denotes the m -th node of l -th layer. After obtaining the distances, we use a softmax function denoted by $\delta(\cdot)$ to normalize their negative values. The softmax function is defined as $\delta_j(a) = \frac{\exp(a_j)}{\sum_{i=1}^N \exp(a_i)}$, where $a \in \mathbb{R}^N$, and $j \in 1, 2, \dots, N$. If $\theta^t = [\theta_1^t, \theta_2^t \dots \theta_N^t]^\top \in \mathbb{R}^N$ is the vectorized form of the distances from all the sources, we set

$$\mathbf{w}_{init}^{(t)} = \delta(-\theta^t) \quad (6)$$

where $\mathbf{w}_{init}^{(t)}$ is the initialization for w . As we shall see, this choice leads to a substantial performance boost compared to random initialization.

(ii) Optimal step size: Since we would like to ensure rapid convergence of optimization in Eqn. 4, we select the optimal step size for gradient descent in the initial stage. Given an initialization $\mathbf{w}_{init}^{(t)}$ and a step size $\alpha^{(t)}$, we compute the second-order Taylor series approximation of the function $\mathcal{L}_w^{(t)}$ at the updated point after one gradient step. Next, we determine the best step size $\alpha_{best}^{(t)}$ by minimizing the approximation with respect to $\alpha^{(t)}$. This is essentially an approximate Newton's method and has a closed-form solution given by

$$\alpha_{best}^{(t)} = \left[\left(\nabla_{\mathbf{w}} \mathcal{L}_w^{(t)} \right)^\top \left(\nabla_{\mathbf{w}} \mathcal{L}_w^{(t)} \right) / \left(\nabla_{\mathbf{w}} \mathcal{L}_w^{(t)} \right)^\top \mathcal{H}_w \left(\nabla_{\mathbf{w}} \mathcal{L}_w^{(t)} \right) \right] \Big|_{\mathbf{w}^{init}}. \quad (7)$$

Here $\nabla_{\mathbf{w}} \mathcal{L}_w^{(t)}$ and \mathcal{H}_w are the gradient and Hessian of $\mathcal{L}_w^{(t)}$ with respect to \mathbf{w} . Together with $\mathbf{w}_{init}^{(t)}$ and $\alpha_{best}^{(t)}$, optimization of (4) converges very quickly as demonstrated in the experiments (in supplementary).

We provide a complete overview of MeTA in Algorithm 1.

Theoretical insights for MeTA

We now provide theoretical justification on how MeTA selects the best source model by optimally trading off model accuracy and domain mismatch. At time t , let $\mathbf{f}_S^{(t)}$ be the set of source models defined as $\left[\mathbf{f}_S^{1(t)} \mathbf{f}_S^{2(t)} \dots \mathbf{f}_S^{N(t)} \right]$. MeTA aims to learn a combination of these models by optimizing weights w on the target domain. For simplicity of exposition, we consider convex combinations $w \in \Delta$ where Δ is the N -dimensional simplex.

To learn $w \in \Delta$, MeTA runs empirical risk minimization on the target task using a loss function $\ell(\cdot)$ with pseudo-labels generated by w -weighted source models. Let $\mathcal{L}(f)$ denote the target population/test risk of a model f (with respect to ground-truth labels) and $\mathcal{L}_T^{*(t)}$ represent the optimal population risk obtained by choosing the best possible $w \in \Delta$ (i.e. oracle risk). We introduce the functions: (1) Ψ which returns the distance between two data distributions and (2) φ which returns the distance between two label distributions. We note that, rather than problem-agnostic metrics like Wasserstein, our Ψ, φ definitions are in terms of the loss landscape and source models $\mathbf{f}_S^{(t)}$, hence tighter. We have the following (informal) generalization bound at time step t (precise details in supplementary).

Theorem 1 (Informal) Consider the model $\mathbf{f}_T^{(t)}$ with combination weights $w^{*(t)}$ obtained via MeTA by minimizing the empirical risk over B IID target examples per Eqn. 5. Let $\hat{y}_w^{(t)}$ denote the pseudo-label variable of w -weighted source models and $\mathcal{D}_w^{(t)} = \sum_{i=1}^N w_i^{(t)} \mathcal{D}_{S_i}^{(t)}$ denote weighted source distribution. Under Lipschitz ℓ and bounded $\mathbf{f}_S^{(t)}$, with probability at least $1 - 3e^{-\tau}$ over the target batch, test risk obeys

$$\underbrace{\mathcal{L}(\mathbf{f}_T^{(t)})}_{MeTA} - \underbrace{\mathcal{L}_T^{*(t)}}_{Optimal} \leq \min_{w \in \Delta} \left\{ \underbrace{\Psi(\mathcal{D}_T^{(t)}, \mathcal{D}_w^{(t)})}_{shift} + \underbrace{\varphi(\hat{y}_w^{(t)}, y_w^{(t)})}_{quality} \right\} + \sqrt{\tilde{\mathcal{O}}((N + \tau)/B)}.$$

Algorithm 1: Overview of MeTA

Input: Pre-trained source models $\{\mathbf{f}_S^j\}_{j=1}^N$, streaming sequential unlabeled test data $\{x_i^{(1)}\}_{i=1}^B \rightarrow \{x_i^{(2)}\}_{i=1}^B \rightarrow \dots \{x_i^{(t)}\}_{i=1}^B \rightarrow \dots$
Output: Optimal inference model for t -th test batch $\mathbf{f}_T^{(t)}$ $\forall t$
Initialization: Assign $\mathbf{f}_S^{j(1)} \leftarrow \mathbf{f}_S^j \forall j$
while $t \geq 1$ **do**
 Set initial $\mathbf{w}_{init}^{(t)}$ using Eqn. (6)
 Set $\alpha_{best}^{(t)}$ using Eqn. (7)
 Solve optimization 4 to get $\mathbf{w}^{*(t)}$
 Infer the test batch t using inference model $\mathbf{f}_T^{(t)}$ using Eqn. (5)
 Find source index k such that $k = \arg \max_{1 \leq j \leq N} \mathbf{w}_j^{*(t)}$
 Update source model $\mathbf{f}_S^{k(t)}$ using any SOTA single source TTA method to get $\overline{\mathbf{f}_S^{k(t)}}$
 for $1 \leq j \leq N$ **do**
 if $j = k$ **then**
 Set $\mathbf{f}_S^{j(t+1)} \leftarrow \overline{\mathbf{f}_S^{j(t)}}$
 else
 Set $\mathbf{f}_S^{j(t+1)} \leftarrow \mathbf{f}_S^{j(t)}$
 end
 end
 end
end

Discussion. In a nutshell, this result shows how MeTA strikes a balance between: (1) Choosing the domain that has the smallest **shift** from target and (2) choosing a source model that has **high-quality** pseudo-labels on its own distribution (i.e. $\hat{y}_w^{(t)}$ matches $y_w^{(t)}$). From our analysis, it's evident that, rather than adapting the source models to the target distribution, if we simply optimize the combination weights to optimize pseudo-labels for inference, the left side excess risk term $(\mathcal{L}(\mathbf{f}_T^{(t)}) - \mathcal{L}_T^{*(t)})$ becomes upper bounded by a relatively modest value: This is because the **shift** and **quality** terms on the right-hand side are optimized with respect to w . We note that $\sqrt{N/B}$ is the generalization risk due to finite samples B and search dimension N .

To further refine this, our immediate objective is to tighten the upper bound. This can be achieved by individually adapting each source model to the current test data, all the while maintaining the optimized w constant. Yet, such an approach isn't ideal since our second goal is to preserve knowledge from the source during continual adaptation. To attain our desired goal, we must relax the upper bound, reducing our search over $w \in \hat{\Delta}$. Here, $\hat{\Delta}$ is the discrete counterpart of the simplex Δ : The elements of $\hat{\Delta}$ are one-hot vectors that has all but one entries zero. The elements of $\hat{\Delta}$ essentially represent discrete model selection. Examining the main terms on the right reveals that: (i) source-target distribution shift and (ii) divergence between ground-truth and pseudo-labels are all minimized when we select the source model with the highest correlation to target. This model, denoted by $\mathbf{f}_S^{*(t)}$, essentially corresponds to the largest entry of $w^{*(t)}$ and presents the

Table 2: **Results on Digits dataset.** We train the source models using four digit datasets to perform inference on the remaining dataset. The column abbreviations correspond to the datasets as follows: ‘MM’ for MNIST-M, ‘MT’ for MNIST, ‘UP’ for USPS, ‘SV’ for SVHN, and ‘SY’ for Synthetic Digits.. The table (reporting % error rate(↓)) shows that X+MeTA outperforms all of the baselines (X-Best) consistently .

	MM	MT	UP	SV	SY	Avg.
Source Worst	80.5	59.4	50.3	88.5	84.8	72.7
Source Best	47.7	2.2	16.8	18.3	6.7	18.3
Tent Worst	84.2	46.9	41.1	90.1	85.4	69.5
Tent Best	45.2	2.3	16.7	14.4	6.7	17.1
Tent + MeTA	37.5	1.9	11.2	14.2	6.7	14.3
EaTA Worst	80.1	48.4	42.6	88.0	83.1	68.4
EaTA Best	47.1	2.7	18.2	18.5	7.2	18.7
EaTA + MeTA	39.5	2.0	11.5	18.0	7.0	15.6
CoTTA Worst	80.0	48.3	42.8	87.9	82.9	68.4
CoTTA Best	47.0	2.8	18.6	18.5	7.2	18.8
CoTTA + MeTA	39.6	2.0	11.7	18.1	7.1	15.7

most stringent upper bound within the $\hat{\Delta}$ search space. Thus, to further minimize the right hand side, the second stage of MeTA adapts $f_S^{*(t)}$ with the current test data. Crucially, besides minimizing the target risk, this step helps avoids forgetting the source because $f_S^{*(t)}$ already does a good job at the target task. Thus, during optimization on target data, $f_S^{*(t)}$ will have small gradient and will not move much, resulting in smaller forgetting. Please refer to the supplementary for more detailed discussion along with the proof of this theorem.

Experiments

We evaluate the effectiveness of our approach on both stationary and dynamic test distribution benchmarks.

Datasets. We demonstrate the efficacy of our approach using both standard domain adaptation benchmarks and those used in continuous test time adaptation. For domain adaptation, we employ the *Digits* and *Office-Home* datasets (Venkateswara et al. 2017). For the dynamic TTA, we utilize *CIFAR-100C* and *CIFAR-10C* (Hendrycks and Dietterich 2019). **Detailed descriptions of these datasets and additional experiments on Office-Home and CIFAR-100C along with some results on segmentation task can be found in the supplementary.**

Baseline Methods. Our baselines are some of the widely used state-of-the-art (SOTA) single source test time adaptation methods: we specifically compare our algorithm with Tent (Wang et al. 2020), CoTTA (Wang et al. 2022b) and EaTA (Niu et al. 2022). To evaluate the adaptation performance, we follow the protocol similar to (Ahmed et al. 2021), where we apply each source model to the test data from a particular test domain individually, which yields X-Best and X-Worst where “X” is the name of the single source adaptation method, representing the highest and lowest performances among the source models adapted using method “X”, respectively. For our algorithm, we extend all of the methods “X” in the multi source setting and call the multi-source counterpart of “X” as “X+MeTA”.

Implementation Details. We use ResNet-18 (He et al. 2016) model for all our experiments. For solving the optimization of Eq. (4), we first initialize the combination weights using

Eq. (6) and calculate the optimal learning rate using Eq. (7). After that, we use 5 iterations to update the combination weights using SGD optimizer and the optimal learning rate. For all the experiments we use a batch size of 128, as used by Tent (Wang et al. 2020). For more details on implementation and experimental setting see supplementary.

Experiments on Digit classification. We first report the results of digit classification in Table 2. Each column of the table represents a test domain dataset. We train four source models on the rest of the digit datasets. For instance, in case of ‘MM’ column ‘MM’ is the test domain which is adapted using four source models trained on ‘MT’, ‘UP’, ‘SV’ and ‘SY’ respectively. We calculate the test error of each incoming test batch and then report the numbers by averaging the error values over all the batches. The table shows that MeTA corresponding to each of the single source methods provides a significant reduction of test error compared to the best single source. This demonstrates that when presented with an incoming test batch, MeTA has the capability to effectively blend all available sources using optimal weights, resulting in superior performance compared to the best single source (on average 3% error reduction than the best source). It is important to note that each test batch in this experiment is drawn from the same stationary distribution, which represents the distribution of the target domain. Another baseline exists that simply uses a naive ensemble of the source models, without any weight optimization. In situations where there’s a significant performance gap between the best and worst source models adapted using single-source methods, a uniform ensemble of these models produces a predictor that trails considerably behind the best-adapted source, as noted by (Ahmed et al. 2021). Referring to Table 2, when testing on the SVHN dataset, the error disparity between the best and worst adapted source models is approximately 70.7%—a substantial margin. Consequently, using a uniform ensemble in such a scenario results in an error rate of roughly 45.5% (experimentally found, not reported in the table). This is strikingly higher than our method’s error rate of around 14.2%. Given these findings, we deduce that uniform ensembling isn’t a reliable approach for model fusion. Thus, we exclude it from our experiment section’s baseline.

Experiments on CIFAR-100C. We conduct a thorough experiment on this dataset to investigate the performance of our model under dynamic test distribution. We consider 3 corruption noises out of 15 noises from CIFAR-100C, which are adversarial weather conditions namely *Snow*, *Fog* and *Frost*. We add these noises for severity level 5 to the original CIFAR-100 training set and train three source models, one for each noise. Along with these models, we also add the model trained on clean training set of CIFAR-100. During testing, we sequentially adapt the models across the 15 noisy domains, each with a severity of 5, from the CIFAR-100C dataset (Wang et al. 2022b; Niu et al. 2022). We report the results for this experiment in Table. 3. Moreover, we also conduct an experiment on CIFAR-10 with the exact same experimental settings as with CIFAR-100. **The results for CIFAR-10C are given in supplementary.**

From the table, we can draw two key observations:
(i) As anticipated, X+MeTA consistently outperforms X-Best

Table 3: **Results on CIFAR-100C.** We take four source models trained on *Clear*, *Snow*, *Fog*, and *Frost*. We employ these models for adaptation on 15 sequential test domains. This table illustrates that even in the dynamic environment X+MeTA performs better than X-Best, which is the direct consequence of optimal aggregation of source models as well as better preservation of source knowledge. (Results in error rate \downarrow (in %))

	GN	SN	IN	DB	GB	MB	ZB	Snow	Frost	Fog	Bright	Contrast	Elastic	Pixel	JPEG	Mean
Source Worst	97.7	96.5	98.2	68.8	78.1	66.1	65.1	53.6	59.3	62.0	55.8	95.4	61.9	71.5	75.2	73.7
Source Best	90.5	89.0	94.5	50.7	48.1	51.9	44.5	30.0	29.5	28.2	39.0	81.9	44.0	38.5	57.1	54.5
Tent Worst	55.9	55.6	71.2	58.0	75.5	78.2	83.3	89.2	92.4	93.7	95.4	96.7	96.5	96.6	96.7	82.3
Tent Best	45.6	43.8	59.1	48.5	59.1	59.1	60.4	65.6	66.1	76.7	75.3	89.8	89.0	91.3	94.2	68.2
Tent + MeTA	42.2	40.6	55.3	28.6	40.7	31.9	29.6	31.7	32.4	30.9	28.6	41.5	38.5	34.8	49.9	37.1
EaTA Worst	57.7	54.0	66.5	40.6	53.2	41.4	36.8	44.0	43.5	45.4	34.8	45.4	45.7	39.9	55.7	47.0
EaTA Best	48.1	44.7	57.9	37.1	44.1	38.7	34.9	33.7	31.9	31.6	33.2	37.2	40.0	34.7	50.3	39.9
EaTA + MeTA	43.3	40.7	54.3	27.5	39.4	30.4	27.5	29.2	29.1	28.3	25.9	31.3	33.4	29.0	43.1	34.2
CoTTA Worst	59.2	57.4	68.0	40.1	52.7	42.1	40.5	47.0	46.6	47.2	39.4	43.6	44.5	41.4	47.4	47.8
CoTTA Best	49.8	46.6	58.6	34.0	40.7	36.5	34.2	34.2	32.8	33.0	32.8	34.8	35.3	33.6	41.1	38.5
CoTTA + MeTA	45.0	44.2	57.7	30.1	38.9	34.0	31.9	33.7	31.5	34.7	30.9	33.0	34.1	32.2	40.9	36.9

across each test distribution, underscoring the validity of our algorithmic proposition. (ii) Given that the CoTTA and EaTA methods are tailored to mitigate forgetting, the average error post-adaptation across the 15 noises using these methods is significantly lower than that of Tent, which isn't designed for this specific challenge. For instance, in Table 3, Tent-Best error is approximately 68.2%, while CoTTA and EaTA-Best are around 39.9% and 38.5%, respectively. However, when these adaptation methods are incorporated into our framework, the final errors are remarkably close: 37.1% for Tent, 34.2% for EaTA, and 36.9% for CoTTA. This suggests that even though Tent is more lightweight and faster compared to the other methods and isn't inherently designed to handle forgetting, its performance within our framework is on par with the results obtained when incorporating the other two methods designed to prevent forgetting. This shows the generalizability of our approach to various single-source methods.

Analysis of Forgetting. Here, we demonstrate the robustness of our method against catastrophic forgetting by evaluating the classification accuracy on the source test set after completing adaptation to each domain (Niu et al. 2022; Song et al. 2023; Chakrabarty, Sreenivas, and Biswas 2023). In the case of MeTA, we use our ensembling method to adapt to the incoming domain. Once the adaptation completes, we infer each of the adapted source models on its corresponding source test set. For the baseline single-source methods, every model is adapted individually to the incoming domain, followed by inference on its corresponding source test set. The accuracy we report represents the average accuracy obtained from each of these single-source adapted models.

From Figure 3, we note that X+MeTA consistently maintains its source accuracy during the adaptation process across the 15 sequential noises. In contrast, the accuracy for each individual single-source method (X) declines on the source test set as the adaptation process progresses. Specifically, Tent, not being crafted to alleviate forgetting, experiences a sharp decline in accuracy. While CoTTA and EaTA exhibit forgetting, it occurs at a slower and more gradual pace. Contrary to all of these single-source methods, our algorithm exhibits virtually no forgetting throughout the process.

Ablation Study. We have performed ablation study with different initialization and learning rate choices for solving the optimization in (4). We also perform experiment to show

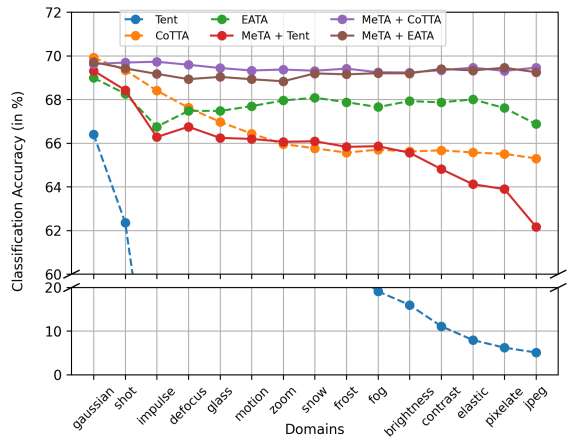


Figure 3: **Comparison with baselines in terms of source knowledge forgetting.** Maintaining the same setting as in Table 3, we demonstrate that by integrating single-source methods with MeTA, the source knowledge is better preserved during dynamic adaptation. Plots without a break in y-axis are provided in the supplementary.

that updating the most correlated model parameters is indeed beneficial (*supplementary material*).

Conclusions and Future work

We propose a novel Test Time Adaptation algorithm, called MeTA, that effectively combines multiple source models during testing to achieve a test accuracy that is at least as good as the best individual source model. In addition, the design of MeTA offers the added benefit of naturally preventing the issue of catastrophic forgetting. To validate the effectiveness of our algorithm, we conduct experiments on a diverse range of benchmark datasets for classification and semantic segmentation tasks. We demonstrate that MeTA can be integrated with a variety of single-source methods. Along these lines, there are several promising future directions to consider. For example, while we currently compute weights for all available sources, it may be worthwhile to investigate if there exists an optimal subset of sources that, when properly weighted, can provide a more optimal solution.

References

Ahmed, S. M.; Lohit, S.; Peng, K.-C.; Jones, M. J.; and Roy-Chowdhury, A. K. 2022. Cross-Modal Knowledge Transfer Without Task-Relevant Source Data. In *Computer Vision–ECCV 2022: 17th European Conference, Tel Aviv, Israel, October 23–27, 2022, Proceedings, Part XXXIV*, 111–127. Springer.

Ahmed, S. M.; Raychaudhuri, D. S.; Paul, S.; Oymak, S.; and Roy-Chowdhury, A. K. 2021. Unsupervised multi-source domain adaptation without access to source data. In *CVPR*.

Chakrabarty, G.; Sreenivas, M.; and Biswas, S. 2023. SATA: Source Anchoring and Target Alignment Network for Continual Test Time Adaptation. *arXiv preprint arXiv:2304.10113*.

Chen, D.; Wang, D.; Darrell, T.; and Ebrahimi, S. 2022. Contrastive test-time adaptation. In *Proceedings of the IEEE/CVF Conference on Computer Vision and Pattern Recognition*, 295–305.

Ding, N.; Xu, Y.; Tang, Y.; Xu, C.; Wang, Y.; and Tao, D. 2022. Source-free domain adaptation via distribution estimation. In *Proceedings of the IEEE/CVF Conference on Computer Vision and Pattern Recognition*, 7212–7222.

Dubey, A.; Ramanathan, V.; Pentland, A.; and Mahajan, D. 2021. Adaptive methods for real-world domain generalization. In *Proceedings of the IEEE/CVF Conference on Computer Vision and Pattern Recognition*, 14340–14349.

Ganin, Y.; Ustinova, E.; Ajakan, H.; Germain, P.; Larochelle, H.; Laviolette, F.; Marchand, M.; and Lempitsky, V. 2016. Domain-adversarial training of neural networks. In *JMLR*.

Guo, J.; Shah, D. J.; and Barzilay, R. 2018. Multi-source domain adaptation with mixture of experts. *arXiv preprint arXiv:1809.02256*.

He, K.; Zhang, X.; Ren, S.; and Sun, J. 2016. Deep residual learning for image recognition. In *Proceedings of the IEEE conference on computer vision and pattern recognition*, 770–778.

Hendrycks, D.; and Dietterich, T. 2019. Benchmarking neural network robustness to common corruptions and perturbations. *arXiv preprint arXiv:1903.12261*.

Hoffman, J.; Tzeng, E.; Park, T.; Zhu, J.-Y.; Isola, P.; Saenko, K.; Efros, A. A.; and Darrell, T. 2018. CyCADA: Cycle-Consistent Adversarial Domain Adaptation. In *ICML*.

Hsu, H.-K.; Yao, C.-H.; Tsai, Y.-H.; Hung, W.-C.; Tseng, H.-Y.; Singh, M.; and Yang, M.-H. 2020. Progressive domain adaptation for object detection. In *WACV*.

Hu, M.; Song, T.; Gu, Y.; Luo, X.; Chen, J.; Chen, Y.; Zhang, Y.; and Zhang, S. 2021. Fully test-time adaptation for image segmentation. In *Medical Image Computing and Computer Assisted Intervention–MICCAI 2021: 24th International Conference, Strasbourg, France, September 27–October 1, 2021, Proceedings, Part III* 24, 251–260. Springer.

Kumar, V.; Lal, R.; Patil, H.; and Chakrabarty, A. 2023. CoNMix for Source-free Single and Multi-target Domain Adaptation. In *WACV*.

Kundu, J. N.; Venkat, N.; Babu, R. V.; et al. 2020. Universal source-free domain adaptation. In *Proceedings of the IEEE/CVF Conference on Computer Vision and Pattern Recognition*, 4544–4553.

Li, R.; Jiao, Q.; Cao, W.; Wong, H.-S.; and Wu, S. 2020. Model adaptation: Unsupervised domain adaptation without source data. In *Proceedings of the IEEE/CVF conference on computer vision and pattern recognition*, 9641–9650.

Li, Y.; Carlson, D. E.; et al. 2018. Extracting relationships by multi-domain matching. *Advances in Neural Information Processing Systems*, 31.

Li, Y.; Wang, N.; Shi, J.; Liu, J.; and Hou, X. 2016. Revisiting batch normalization for practical domain adaptation. *arXiv preprint arXiv:1603.04779*.

Liang, J.; Hu, D.; and Feng, J. 2020. Do we really need to access the source data? source hypothesis transfer for unsupervised domain adaptation. In *ICML*.

Liu, Y.; Zhang, W.; and Wang, J. 2021. Source-free domain adaptation for semantic segmentation. In *Proceedings of the IEEE/CVF Conference on Computer Vision and Pattern Recognition*, 1215–1224.

Long, M.; Cao, Y.; Wang, J.; and Jordan, M. 2015. Learning transferable features with deep adaptation networks. In *ICML*.

Mirza, M. J.; Micorek, J.; Possegger, H.; and Bischof, H. 2022. The norm must go on: dynamic unsupervised domain adaptation by normalization. In *Proceedings of the IEEE/CVF Conference on Computer Vision and Pattern Recognition*, 14765–14775.

Niu, S.; Wu, J.; Zhang, Y.; Chen, Y.; Zheng, S.; Zhao, P.; and Tan, M. 2022. Efficient test-time model adaptation without forgetting. In *International conference on machine learning*, 16888–16905. PMLR.

Peng, X.; Bai, Q.; Xia, X.; Huang, Z.; Saenko, K.; and Wang, B. 2019. Moment matching for multi-source domain adaptation. In *Proceedings of the IEEE/CVF international conference on computer vision*, 1406–1415.

Raychaudhuri, D. S.; Paul, S.; Vanbaar, J.; and Roy-Chowdhury, A. K. 2021. Cross-domain imitation from observations. In *ICML*.

Shin, I.; Tsai, Y.-H.; Zhuang, B.; Schulter, S.; Liu, B.; Garg, S.; Kweon, I. S.; and Yoon, K.-J. 2022. MM-TTA: multi-modal test-time adaptation for 3d semantic segmentation. In *Proceedings of the IEEE/CVF Conference on Computer Vision and Pattern Recognition*, 16928–16937.

Song, J.; Lee, J.; Kweon, I. S.; and Choi, S. 2023. EcoTTA: Memory-Efficient Continual Test-time Adaptation via Self-distilled Regularization. In *Proceedings of the IEEE/CVF Conference on Computer Vision and Pattern Recognition*, 11920–11929.

Tran, L.; Sohn, K.; Yu, X.; Liu, X.; and Chandraker, M. 2019. Gotta Adapt 'Em All: Joint Pixel and Feature-Level Domain Adaptation for Recognition in the Wild. In *CVPR*.

Tsai, Y.-H.; Hung, W.-C.; Schulter, S.; Sohn, K.; Yang, M.-H.; and Chandraker, M. 2018. Learning to Adapt Structured Output Space for Semantic Segmentation. In *CVPR*.

Tzeng, E.; Hoffman, J.; Saenko, K.; and Darrell, T. 2017. Adversarial discriminative domain adaptation. In *CVPR*.

Valanarasu, J. M. J.; Guo, P.; VS, V.; and Patel, V. M. 2022. On-the-Fly Test-time Adaptation for Medical Image Segmentation. *arXiv preprint arXiv:2203.05574*.

Venkateswara, H.; Eusebio, J.; Chakraborty, S.; and Panchanathan, S. 2017. Deep hashing network for unsupervised domain adaptation. In *Proceedings of the IEEE conference on computer vision and pattern recognition*, 5018–5027.

Wang, D.; Shelhamer, E.; Liu, S.; Olshausen, B.; and Darrell, T. 2020. Tent: Fully test-time adaptation by entropy minimization. *arXiv preprint arXiv:2006.10726*.

Wang, F.; Han, Z.; Gong, Y.; and Yin, Y. 2022a. Exploring domain-invariant parameters for source free domain adaptation. In *Proceedings of the IEEE/CVF Conference on Computer Vision and Pattern Recognition*, 7151–7160.

Wang, Q.; Fink, O.; Van Gool, L.; and Dai, D. 2022b. Continual test-time domain adaptation. In *Proceedings of the IEEE/CVF Conference on Computer Vision and Pattern Recognition*, 7201–7211.

Xia, H.; Zhao, H.; and Ding, Z. 2021. Adaptive Adversarial Network for Source-Free Domain Adaptation. In *ICCV*.

Xiao, Z.; Zhen, X.; Shao, L.; and Snoek, C. G. 2022. Learning to generalize across domains on single test samples. *arXiv preprint arXiv:2202.08045*.

Xu, R.; Chen, Z.; Zuo, W.; Yan, J.; and Lin, L. 2018. Deep cocktail network: Multi-source unsupervised domain adaptation with category shift. In *Proceedings of the IEEE conference on computer vision and pattern recognition*, 3964–3973.

Yang, S.; Wang, Y.; Van De Weijer, J.; Herranz, L.; and Jui, S. 2020. Unsupervised domain adaptation without source data by casting a bait. *arXiv preprint arXiv:2010.12427*, 1(2): 5.

Yang, S.; Wang, Y.; Van De Weijer, J.; Herranz, L.; and Jui, S. 2021. Generalized source-free domain adaptation. In *Proceedings of the IEEE/CVF International Conference on Computer Vision*, 8978–8987.

Ye, H.; Xie, Q.; and Ng, H. T. 2023. Multi-Source Test-Time Adaptation as Dueling Bandits for Extractive Question Answering. *arXiv preprint arXiv:2306.06779*.

Yeh, H.-W.; Yang, B.; Yuen, P. C.; and Harada, T. 2021. SoFA: Source-Data-Free Feature Alignment for Unsupervised Domain Adaptation. In *WACV*.

Zhao, S.; Li, B.; Xu, P.; and Keutzer, K. 2020. Multi-source domain adaptation in the deep learning era: A systematic survey. *arXiv preprint arXiv:2002.12169*.

MeTA: Multi-source Test Time Adaptation (Supplementary Material)

Office-Home

Here we put the results of the experiments on Office-Home.

Table 1: Results on Office-Home. We train three source models using three domains in this dataset and use them for inference on the remaining domain under the TTA setting. Our results demonstrate that X+MeTA consistently outperforms all of the baselines (X) (% error).

	Ar	Cl	Pr	Rw	Avg.
Source Worst	61.4	64.9	46.2	43.9	54.1
Source Best	42.5	58.5	29.8	35.7	41.6
Tent Worst	57.7	60.4	46.5	42.1	51.7
Tent Best	41.4	54.3	27.9	36.0	39.9
Tent + MeTA	40.7	52.5	27.4	27.4	37.0
EaTA Worst	58.4	64.3	48.0	43.5	53.5
EaTA Best	42.1	57.8	30.3	35.9	41.5
EaTA + MeTA	40.1	53.3	28.3	28.0	37.4
CoTTA Worst	58.3	62.9	47.1	42.8	52.8
CoTTA Best	42.1	55.0	29.0	34.9	40.2
CoTTA + MeTA	40.6	53.3	28.3	29.0	37.8

In the table, the column refers to the target distribution. Three source models are trained on the rest of the distributions. It can be observed here that X+MeTA consistency yields better than best source performance.

CIFAR-10C

Note that identical to the experiment on CIFAR-100 in the main paper the results on CIFAR-10 follow the same trend where X+MeTA outperforms the X-Best.

In the single-source scenario, one among the four source models achieves the X-Best (for example CoTTA-Best) accuracy for a specific domain. The determination of which individual model (from the four) will attain the best accuracy for that domain remains uncertain beforehand. Furthermore, the individual source model yielding the X-Best accuracy varies across different domains within CIFAR10-C. However, in our X+MeTA approach, the need to deliberate over the selection of one out of the four source models is eliminated. X+MeTA reliably outperforms any single source X-model that might achieve the X-Best accuracy.

Individual TTA methods may have distinct advantages. For example, Tent offers several distinct advantages over

CoTTA, including its lightweight nature and faster performance. Conversely, CoTTA presents certain benefits over Tent, such as increased resilience against forgetting. Consequently, the choice between TTA methods is dependent on the user's preferences, aligning with the specific task at hand. In this experiment, we have demonstrated that MeTA can be integrated with any TTA method of the user's choosing.

Ablation Study

Table 4 of supplementary presents the error rate results on the Office-Home dataset under the same experimental setting as Table 1 (supplementary) with Tent as the adaptation method, but with different initialization and learning rate choices for solving the optimization in (6). It is evident from the table that our chosen initialization and adaptive learning rate result in the highest accuracy gain. In Table 3, we demonstrate that by updating only the model with the highest correlation to the test domain, our method produces the lowest test accuracy. This is in comparison to scenarios where we either update all models or solely the least correlated one. This empirical observation directly supports our theoretical assertion from the theorem: updating the most correlated model is most effective in preventing forgetting, thereby resulting in the smallest test error during gradual adaptation.

Implementation Details

In this section, we provide a comprehensive overview of our experimental setup. We conducted two sets of experiments: one on a stationary target distribution, and the other on a dynamic target distribution that changes continuously.

Stationary Target

Digit Classification The digit classification task consists of five distinct domains from which we construct five different adaptation scenarios. Each scenario involves four source models, with the remaining domain treated as the target distribution. In total, we construct five adaptation scenarios for our study.

The ResNet-18 architecture was used for all models, with an image size of 64×64 and a batch size of 128 during testing. Mean accuracy over the entire test set is reported in Table 2 of the main paper. For Tent we use a learning rate of 0.01 and for rest of the adaptation method a learning rate of

Table 2: **Results on CIFAR-10C.** We take four source models trained on *Clear*, *Snow*, *Fog* and *Frost*. We employ these models for adaptation on 15 sequential test domains. This table illustrates that even in the dynamic environment X+MeTA performs better than X+, which is the direct consequence of better retaining source knowledge. (Results in error rate \downarrow (in %))

	GN	SN	IN	DB	GB	MB	ZB	Snow	Frost	Fog	Bright	Contrast	Elastic	Pixel	JPEG	Mean
Source Worst	84.7	81.1	89.1	42.6	55.6	36.2	32.2	30.6	39.2	28.7	18.5	76.4	26.9	50.0	32.7	48.3
Source Best	72.1	67.8	76.5	22.8	20.4	26.6	18.7	8.1	8.2	6.9	10.6	56.8	18.8	13.9	23.9	30.1
Tent Worst	26.6	22.7	36.1	20.0	34.9	28.8	28.7	32.8	34.4	36.1	30.3	38.2	44.8	41.7	46.8	33.5
Tent Best	19.3	17.6	27.9	14.5	21.1	17.6	13.5	14.3	12.6	14.4	12.4	17.0	19.0	14.3	20.4	17.1
Tent + MeTA	17.2	15.6	25.7	9.1	19.1	11.7	9.0	9.9	10.1	9.7	7.7	11.7	14.5	10.3	17.4	13.2
EaTA Worst	31.5	30.4	44.8	14.8	33.9	16.1	13.4	20.5	21.6	19.3	11.2	18.9	23.2	19.5	29.6	23.2
EaTA Best	21.9	20.8	33.9	10.5	19.6	14.3	10.6	8.6	9.0	7.5	8.5	10.3	16.1	11.4	24.0	15.1
EaTA + MeTA	18.0	17.3	29.4	8.3	18.2	10.0	7.5	8.0	8.4	7.9	6.4	9.1	13.1	10.0	18.1	12.6
CoTTA Worst	30.1	26.8	37.8	15.0	28.5	16.6	14.6	19.3	18.6	17.5	12.2	15.9	19.4	15.4	19.3	20.5
CoTTA Best	21.0	18.5	28.0	11.2	17.3	13.3	11.1	10.6	10.4	9.5	9.7	11.2	13.1	10.5	15.6	14.1
CoTTA + MeTA	18.4	17.0	28.0	8.4	17.7	10.7	7.9	9.1	8.4	8.5	6.8	8.3	12.1	9.3	15.3	12.4

Table 3: **Choice of model update.** In our experiments using Tent as the model update method on CIFAR-100, we tested three scenarios: updating all models, updating only the least correlated model, and updating only the most correlated model. Our results indicate that our model selection approach produces the most favorable outcome.

Update Policy	GN	SN	IN	DB	GB	MB	ZB	Snow	Frost	Fog	Bright	Contrast	Elastic	Pixel	JPEG	Mean
All Model Update	41.6	40.9	57.8	47.1	60.2	60.3	62.1	68.6	73.2	80.9	82.1	92.4	91.2	92.5	94.9	69.7
Least Corr. Update	43.8	41.4	56.1	31.2	41.4	34.8	31.4	33.5	33.1	37.5	31.5	41.6	41.5	37.5	53.1	39.3
Most Corr. Update	42.2	40.6	55.3	28.6	40.7	31.9	29.6	31.7	32.4	30.9	28.6	41.5	38.5	34.8	49.9	37.1

Table 4: **Effect of initialization and step size choice.** Error rate on Office-Home under different choices of initialization and step sizes.

Initialization	Step size					
	1e - 3	1e - 2	1e - 1	1e0	1e1	Ours
Random	40.7	40.9	40.6	39.6	41.5	39.3
Ours	37.9	37.8	37.5	37.4	39.1	37.0

0.001 is used. We use Adam optimizer for all the adaptation methods. Model parameter update is performed using a single step of gradient descent.

Object Recognition The object recognition task on the Office-Home dataset comprises of four distinct domains from which we construct four different adaptation scenarios, similar to the digit classification setup. We use the same experimental settings and hyperparameters as the digit classification experiment, with the exception of the image size, which is set to 224×224 in this experiment. The results of this evaluation are reported in Table 3 of the main paper.

Dynamic Target

CIFAR-10/100-C In this experiment, we use four ResNet-18 source models trained on different variants of the CIFAR-10/100 dataset: 1) vanilla train set, 2) train set with added fog (severity = 5), 3) train set with added snow (severity = 5), and 4) train set with added frost (severity = 5). To evaluate the models, we use the test set of CIFAR-10/100C (severity = 5) and adapt to each of the domains in a continual manner. The images are resized to 224×224 . For all the adaptation methods, a learning rate of 0.001 with Adam optimizer is used.

Semantic Segmentation

Our method is not just limited to image classification tasks and can be easily extended to other tasks like semantic segmentation (sem-seg). We assume access to a set of sem-seg source models $\{f_S^j\}_{j=1}^N$, where each model classifies every pixel of an input image to some class. Specifically, $f_S^j : \mathbb{R}^{H \times W} \rightarrow \mathbb{R}^{H \times W \times K}$, where K is the number of classes. In this case, the entropy in Eqn. 3 of the main paper will be modified as follows:

$$\mathcal{L}_w^{(t)}(\mathbf{w}) = -\mathbb{E}_{\mathcal{D}_T^{(t)}} \sum_{h=1}^H \sum_{w=1}^W \sum_{c=1}^K \hat{y}_{ihwc}^{(t)} \log(\hat{y}_{ihwc}^{(t)}) \quad (1)$$

Where, $\hat{y}_{ihwc}^{(t)}$ is the weighted probability output corresponding to class c for the pixel at location (h, w) at timestamp t . We modify Eqn. 3 in the main paper, while keeping the rest of the framework the same.

Datasets

We use the following datasets in our experiments:

- **Cityscapes:** Cityscapes (Cordts et al. 2016) is a large-scale dataset that has dense pixel-level annotations for 30 classes grouped into 8 categories (flat surfaces, humans, vehicles, constructions, objects, nature, sky, and void). There are also fog and rain variants (Sakaridis et al. 2018; Hu et al. 2019) of the Cityscapes dataset, where the clean images of Cityscapes have been simulated to add fog and rainy weather conditions.
- **ACDC:** The Adverse Conditions Dataset (Sakaridis, Dai, and Van Gool 2021) has images corresponding to fog, nighttime, rain, and snow weather conditions. Also, the corresponding pixel-level annotations are available. The number of classes is the same as the evaluation classes of the Cityscapes dataset.

Table 5: **Result on Cityscape to ACDC:** In this experiment, we test our method on the test data from individual weather conditions (static test distribution) of ACDC. The source models are trained on the train set of Cityscape and its noisy variants. Our method clearly outperforms baseline adaptation method. (Results in % mIoU)

Method	Fog	Rain	Snow	Night	Avg.
Tent-Best	25.3	21.0	19.2	12.6	19.5
MeTA	27.7	22.8	21.1	14.0	21.4

Table 6: **Result on Cityscapes to ACDC for dynamic test distribution:** This table illustrates that over a prolonged cycle of repetitive test distributions, our model can retain performance better than baseline Tent. ((Results in % mIoU))

Time	t				3				5				All
Round	1				3				5				Mean
Conditions	Rain	Snow	Fog	Night	Rain	Snow	Fog	Night	Rain	Snow	Fog	Night	Mean
Tent-Best	20.1	21.3	22.3	11.3	18.5	17.2	19.5	8.4	15.8	14.5	17.5	6.8	16.1
MeTA	22.1	21.4	24.3	13.4	21.4	18.3	23.5	11.3	18.6	15.5	21.4	10.4	18.6

Experimental setup

We use Deeplab v3+ (Chen et al. 2018) with a ResNet-18 encoder as the segmentation model for all the experiments. We resize the input images to a size of 512×512 . Following the conventional evaluation protocol (Cordts et al. 2016), we evaluate our model on 19 semantic labels without considering the void label.

We first experiment in a static target distribution setting. Specifically, we train three source models on clean, fog, and rain train splits of Cityscapes. We then evaluate the models on the test set of each of the weather conditions of ACDC dataset using MeTA and baseline Tent models. We use a batch size of 16 and report the mean accuracy over all the test batches. Again, we have updated the combination weights of MeTA with SGD optimizer using 5 iterations. For updating the source model in MeTA that has the most correlation with the incoming test batch, we use the Adam optimizer with a learning rate of 0.001 and updated the batch-norm parameters with one iteration. The baseline Tent models are also updated with the same optimizer and learning rate. The results in Table. 5 clearly demonstrate that MeTA outperforms all the baselines on test data from each of the adverse weather conditions.

We also evaluate our method in a dynamic test distribution setting, where we have sequentially incoming test batches from the four weather condition test sets of ACDC dataset. The test sequence includes 5 batches of Rain, followed by 5 batches of Snow, 5 batches of Fog, and finally 5 batches of Night. This sequence is repeated (with the same test images) for a total of 5 rounds. We report the mean accuracy over the 5 batches and include the results for the 1st, 3rd, and 5th rounds in Table 6. We use the same hyperparameters as in the dynamic setting of previous experiments with the exception that the batch-size is 16.

Visualization

In Fig. 1, we present the input images along with the corresponding predicted masks of the baseline models and MeTA from the last round. The figure contains rows of input image samples from the four different weather conditions of

the ACDC dataset, in the order of rain, snow, fog, and night. MeTA is compared with baseline adaptation method Tent, and as shown in Fig. 1, it is evident that MeTA provides better segmentation results compared to the baselines visually.

Proof and discussion of Theorem 1

Theorem 1 (Informal). Consider the model $f_T^{(t)}$ with combination weights $w^{*(t)}$ obtained via MeTA by minimizing the empirical risk over B IID target examples per Eqn. 5 (main paper). Let $\hat{y}_w^{(t)}$ denote the pseudo-label variable of w -weighted source models and $\mathcal{D}_w^{(t)} = \sum_{i=1}^N w_i^{(t)} \mathcal{D}_{S_i}^{(t)}$ denote weighted source distribution. Under Lipschitz ℓ and bounded $f_S^{(t)}$, with probability at least $1 - 3e^{-\tau}$ over the target batch, test risk obeys

$$\begin{aligned} \mathcal{L}(f_T^{(t)}) - \mathcal{L}_T^{*(t)} &\leq \min_{w \in \Delta} \{\Psi(\mathcal{D}_T^{(t)}, \mathcal{D}_w^{(t)}) + \varphi(\hat{y}_w^{(t)}, y_w^{(t)})\} \\ &\quad + \sqrt{\tilde{\mathcal{O}}((N + \tau)/B)}. \end{aligned}$$

Proof. We adapt the theorem from a corollary (corollary 1) in (Oymak, Li, and Soltanolkotabi 2021). In this corollary the following result was derived:

$$\begin{aligned} \mathcal{L}(f_{\hat{\alpha}}^{\tau}) &\leq \min_{\alpha \in \Delta} (l_{\star}^{\alpha}(\mathcal{D}) + \text{DM}_{\mathcal{D}'}^{\mathcal{D}}(\alpha) + 4\Gamma\mathcal{R}_{n_{\tau}}(\mathcal{F}_{\alpha})) \\ &\quad + \sqrt{\tilde{\mathcal{O}}((h_{\text{eff}} + t)/n_{\nu})} + \delta \end{aligned}$$

Here f^{τ} in the $f_{\hat{\alpha}}^{\tau}$ is the trained model on the training(τ) distribution \mathcal{D}' and $\hat{\alpha}$ is a hyper-parameter that has been empirically optimized by fine tuning on the validation(ν) distribution \mathcal{D} . \mathcal{L} is the expected risk over the distribution \mathcal{D} . DM measures the distribution mismatch via difference of sub-optimality gap using the training and validation distribution. $\mathcal{R}_{n_{\tau}}(\mathcal{F}_{\alpha})$ is the Rademacher complexity of the function class \mathcal{F} with α as the hyper-parameter. The corollary holds for probability of at least $1 - 3e^{-t}$ and h_{eff} is the effective

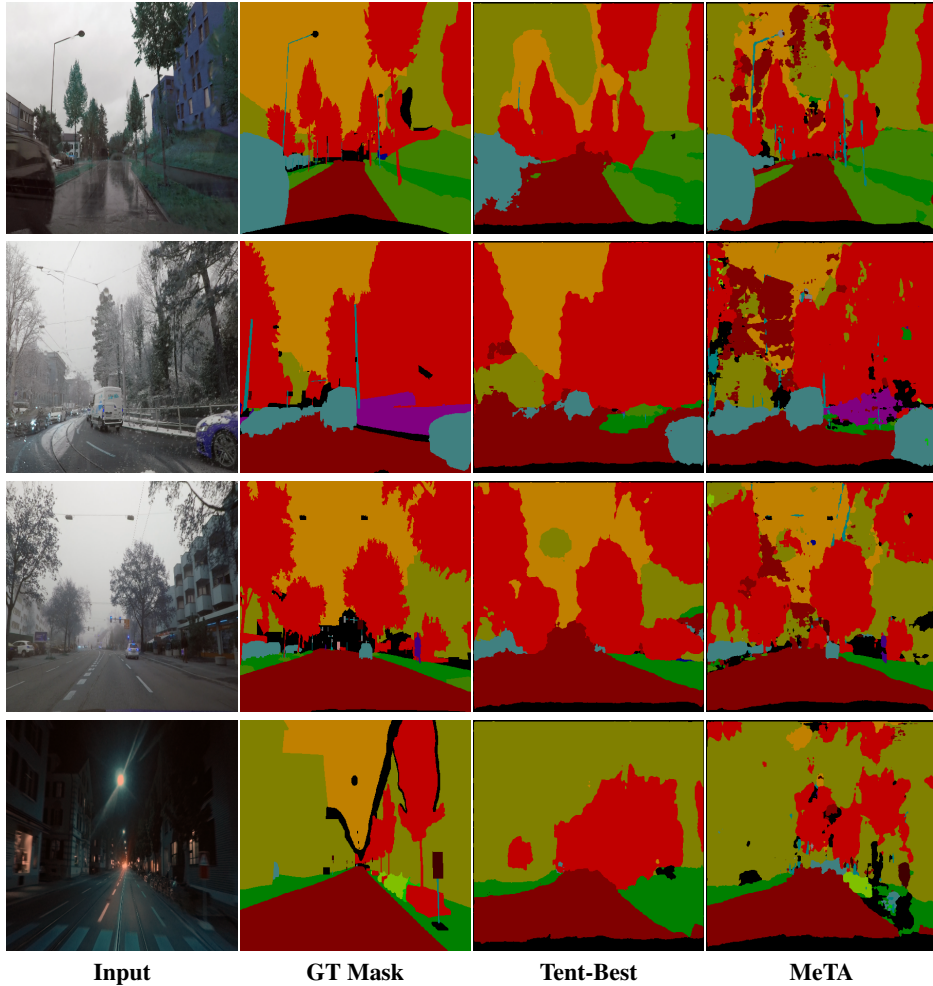


Figure 1: **Visual Comparison of MeTA with Baselines for Semantic Segmentation Task.** Each row in the figure corresponds to a different weather condition (rain, snow, fog, and night from top to bottom). It is evident that MeTA outperforms the baselines in terms of segmentation results.

dimension of the hyper-parameter space. Also n_ν is the number of samples under the validation. The bound can be first of all easily extended to the source/target scenario instead of train/validation. In our scenario the source models jointly construct the function class \mathcal{F}_α where, the hyper-parameter α is the combination weight w . Effective dimension for our case is exactly the number of source model N and instead of t we took τ as the probability variable. For the sake of simplicity we omitted $\delta > 0$ which is a positive constant along with the Rademacher complexity. Also $n_\nu = B$ in our setting since we have B number of samples for the target/validation. Now there is a new term in our bound which is φ which was not in the original corollary. This term is used to account for the mismatch between actual and pseudo-labels generated by the source. This is done due to the fact that we do empirical minimization of the entropy of the target pseudo-label since the problem is unsupervised and actual labels are not available. The left side of the inequality is derived using the test/target pseudo-label. Consequently, we can introduce an added

distribution mismatch term. This term can be broken down into three components: mismatch from target pseudo to target ground truth (gt), from target gt to source gt, and from source gt to source pseudo label. Of these components, the first two can be readily integrated into the $\Psi(\cdot)$ function, given that it measures the discrepancy between the weighted source and the target. The remaining third component is denoted by the $\varphi(\cdot)$ function. This completes the proof. \square

Additional discussion

The $\varphi(\cdot)$ function implies that trained sources should produce **high-quality** pseudo-labels within their own distribution. Essentially, this function evaluates the effectiveness of the model's training. For instance, even if the **shift** between the source and target is minimal, a poorly trained source model might still under-perform on the target. Observe that both the **shift** and the **quality** terms are minimized when we broaden our search space over $\hat{\Delta}$. This allows us to select a model that exhibits the highest correlation with the test domain, thereby

providing us with the most strict bound within the discrete simplex.

Examining the issue through the lens of the gradient provides another perspective. By updating the source model that is most correlated with the test data, its gradient will be smaller than those of other models. Over time, this ensures that the model's parameters remain closer to the original source parameters, thereby preventing catastrophic forgetting. Let's examine a toy case mathematically of the most correlated source can give us least gradient.

Let us assume a binary classification task with linear regression where the final activation is sigmoid $\sigma(\cdot)$ function. Now let's take the pseudo-label for a sample x be \hat{y} , where $\hat{y} = \sigma(w^\top x)$. Then the entropy h of \hat{y} will be $h = -\hat{y} \log(\hat{y})$. Then we take the derivative of the objective h w.r.t w weight as follows:

$$\begin{aligned} h &= -\hat{y} \log(\hat{y}) \\ \Rightarrow \frac{\partial h}{\partial w} &= (1 + \log(\hat{y}))\hat{y}(\hat{y} - 1)x \end{aligned}$$

Now we can easily verify that if the source model is closest to the test domain, then the pseudo-label generated by the model has very small entropy which also means \hat{y} is either close to 0 or close to 1. For both of the cases the derivative expression above goes close to zero which validate the claim of having smallest gradient for highest correlated source.

KL divergence between two univariate Gaussians

During the discussion of initialization of the combination weights in Section 3.5, we come up with θ_j^t which is calculated using the formula for KL divergence between two univariate Gaussians $\mathcal{N}(\mu_1, \sigma_1^2)$ and $\mathcal{N}(\mu_2, \sigma_2^2)$. In this section, we provide the detailed derivation of this below:

From the definition of KL divergence, we know the distance between two distributions p and q is given by,

$$\begin{aligned}\mathcal{D}_{KL}(p, q) &= \int_{-\infty}^{+\infty} p(x) \log \left(\frac{p(x)}{q(x)} \right) dx \\ &= \int_{-\infty}^{+\infty} p(x) \log(p(x)) dx - \int_{-\infty}^{+\infty} p(x) \log(q(x)) dx\end{aligned}\tag{2}$$

Here in this problem p and q are univariate Gaussians and can be expressed as follows:

$$p(x) = \frac{1}{(2\pi\sigma_1^2)^{\frac{1}{2}}} \exp \left(-\frac{(x - \mu_1)^2}{2\sigma_1^2} \right), \quad q(x) = \frac{1}{(2\pi\sigma_2^2)^{\frac{1}{2}}} \exp \left(-\frac{(x - \mu_2)^2}{2\sigma_2^2} \right).$$

Now we compute the second term in Eqn. (2) as follows:

$$\begin{aligned}\int_{-\infty}^{+\infty} p(x) \log(q(x)) dx &= \log \left(\frac{1}{(2\pi\sigma_2^2)^{\frac{1}{2}}} \right) - \int_{-\infty}^{+\infty} p(x) \frac{(x - \mu_2)^2}{2\sigma_2^2} dx \\ &= \log \left(\frac{1}{(2\pi\sigma_2^2)^{\frac{1}{2}}} \right) - \frac{\int_{-\infty}^{+\infty} x^2 p(x) dx - 2\mu_2 \int_{-\infty}^{+\infty} x p(x) dx + \mu_2^2}{2\sigma_2^2} \\ &= \log \left(\frac{1}{(2\pi\sigma_2^2)^{\frac{1}{2}}} \right) - \frac{\mathbb{E}[X^2] - 2\mu_2 \mathbb{E}[X] + \mu_2^2}{2\sigma_2^2} \\ &= \log \left(\frac{1}{(2\pi\sigma_2^2)^{\frac{1}{2}}} \right) - \frac{\text{Var}[X] + (\mathbb{E}[X])^2 - 2\mu_2 \mathbb{E}[X] + \mu_2^2}{2\sigma_2^2} \\ &= \log \left(\frac{1}{(2\pi\sigma_2^2)^{\frac{1}{2}}} \right) - \frac{\sigma_1^2 + \mu_1^2 - 2\mu_2 \mu_1 + \mu_2^2}{2\sigma_2^2} \\ &= \log \left(\frac{1}{(2\pi\sigma_2^2)^{\frac{1}{2}}} \right) - \frac{\sigma_1^2 + (\mu_1 - \mu_2)^2}{2\sigma_2^2}\end{aligned}\tag{3}$$

In a similar manner we calculate the first term in Eqn. (2) as follows:

$$\begin{aligned}\int_{-\infty}^{+\infty} p(x) \log(p(x)) dx &= \log \left(\frac{1}{(2\pi\sigma_1^2)^{\frac{1}{2}}} \right) - \int_{-\infty}^{+\infty} p(x) \frac{(x - \mu_1)^2}{2\sigma_1^2} dx \\ &= \log \left(\frac{1}{(2\pi\sigma_1^2)^{\frac{1}{2}}} \right) - \frac{\int_{-\infty}^{+\infty} x^2 p(x) dx - 2\mu_1 \int_{-\infty}^{+\infty} x p(x) dx + \mu_1^2}{2\sigma_1^2} \\ &= \log \left(\frac{1}{(2\pi\sigma_1^2)^{\frac{1}{2}}} \right) - \frac{\mathbb{E}[X^2] - 2\mu_1 \mathbb{E}[X] + \mu_1^2}{2\sigma_1^2} \\ &= \log \left(\frac{1}{(2\pi\sigma_1^2)^{\frac{1}{2}}} \right) - \frac{\text{Var}[X] + (\mathbb{E}[X])^2 - 2\mu_1 \mathbb{E}[X] + \mu_1^2}{2\sigma_1^2} \\ &= \log \left(\frac{1}{(2\pi\sigma_1^2)^{\frac{1}{2}}} \right) - \frac{\sigma_1^2 + \mu_1^2 - 2\mu_1^2 + \mu_1^2}{2\sigma_1^2} \\ &= \log \left(\frac{1}{(2\pi\sigma_1^2)^{\frac{1}{2}}} \right) - \frac{1}{2}\end{aligned}\tag{4}$$

Now combining Eqn. (4) and Eqn. (3), we get the final KL divergence as follows:

$$\begin{aligned}
\mathcal{D}_{KL}(p, q) &= \log \left(\frac{1}{(2\pi\sigma_1^2)^{\frac{1}{2}}} \right) - \frac{1}{2} - \log \left(\frac{1}{(2\pi\sigma_2^2)^{\frac{1}{2}}} \right) + \frac{\sigma_1^2 + (\mu_1 - \mu_2)^2}{2\sigma_2^2} \\
&= \log \left(\frac{\sigma_2}{\sigma_1} \right) + \frac{\sigma_1^2 + (\mu_1 - \mu_2)^2}{2\sigma_2^2} - \frac{1}{2}
\end{aligned} \tag{5}$$

Optimal step size in approximate Newton's method

In the main paper, we compute the optimal combination weights by solving the optimization below:

$$\begin{aligned}
&\underset{\mathbf{w}}{\text{minimize}} \quad \mathcal{L}_w^{(t)}(\mathbf{w}) \\
&\text{subject to} \quad w_j \geq 0, \forall j \in \{1, 2, \dots, N\}, \\
&\quad \sum_{j=1}^n w_j = 1
\end{aligned} \tag{6}$$

To solve this problem, we begin by initializing $\mathbf{w}_{init}^{(t)}$ as $\delta(-\theta^t)$. Next, we determine the optimal step size based on the initial combination weights to minimize the loss $\mathcal{L}_w^{(t)}$ as much as possible. Specifically, we use a second-order Taylor expansion to approximate the loss at the updated point after taking a single step with a step size of $\alpha^{(t)}$. Thus, after one step of gradient descent, the updated point becomes:

$$\mathbf{w}_{init}^{(t)(1)} = \mathbf{w}_{init}^{(t)} - \alpha^{(t)} \left(\nabla_{\mathbf{w}} \mathcal{L}_w^{(t)} \right) \Big|_{\mathbf{w}^{init}} \tag{7}$$

For notational simplicity let us first denote $\mathbf{w}_{init}^{(t)(1)} = \mathbf{w}^{(1)}$, $\mathbf{w}_{init}^{(t)} = \mathbf{w}^{(0)}$ and $\left(\nabla_{\mathbf{w}} \mathcal{L}_w^{(t)} \right) \Big|_{\mathbf{w}^{init}} = \nabla_{\mathbf{w}^{(0)}} \mathcal{L}_w^{(t)}$. We also denote the hessian of $\mathcal{L}_w^{(t)}$ at $\mathbf{w}^{(0)}$ as $\mathcal{H}_{\mathbf{w}^{(0)}}$. Now, we can write the taylor series expansion of $\mathcal{L}_w^{(t)}$ at $\mathbf{w}^{(1)}$ as follows:

$$\begin{aligned}
\mathcal{L}_w^{(t)}(\mathbf{w}^{(1)}) &= \mathcal{L}_w^{(t)}(\mathbf{w}^{(0)} - \alpha^{(t)} \nabla_{\mathbf{w}^{(0)}} \mathcal{L}_w^{(t)}) \\
&= \mathcal{L}_w^{(t)}(\mathbf{w}^{(0)}) - \alpha^{(t)} \left(\nabla_{\mathbf{w}^{(0)}} \mathcal{L}_w^{(t)} \right)^{\top} \left(\nabla_{\mathbf{w}^{(0)}} \mathcal{L}_w^{(t)} \right) + \frac{(\alpha^{(t)})^2}{2} \left(\nabla_{\mathbf{w}^{(0)}} \mathcal{L}_w^{(t)} \right)^{\top} \mathcal{H}_{\mathbf{w}^{(0)}} \left(\nabla_{\mathbf{w}^{(0)}} \mathcal{L}_w^{(t)} \right) + \mathcal{O}((\alpha^{(t)})^3) \\
&\approx \mathcal{L}_w^{(t)}(\mathbf{w}^{(0)}) - \alpha^{(t)} \left(\nabla_{\mathbf{w}^{(0)}} \mathcal{L}_w^{(t)} \right)^{\top} \left(\nabla_{\mathbf{w}^{(0)}} \mathcal{L}_w^{(t)} \right) + \frac{(\alpha^{(t)})^2}{2} \left(\nabla_{\mathbf{w}^{(0)}} \mathcal{L}_w^{(t)} \right)^{\top} \mathcal{H}_{\mathbf{w}^{(0)}} \left(\nabla_{\mathbf{w}^{(0)}} \mathcal{L}_w^{(t)} \right)
\end{aligned} \tag{8}$$

In order to minimize $\mathcal{L}_w^{(t)}(\mathbf{w}^{(1)})$ we differentiate Eqn. (8) with respect to $\alpha^{(t)}$ and set it zero to get $\alpha_{best}^{(t)}$. Specifically,

$$\begin{aligned}
&\frac{\partial \mathcal{L}_w^{(t)}(\mathbf{w}^{(1)})}{\partial \alpha^{(t)}} \Big|_{\alpha^{(t)}=\alpha_{best}^{(t)}} = 0 \\
&\implies - \left(\nabla_{\mathbf{w}^{(0)}} \mathcal{L}_w^{(t)} \right)^{\top} \left(\nabla_{\mathbf{w}^{(0)}} \mathcal{L}_w^{(t)} \right) + \alpha_{best}^{(t)} \left(\nabla_{\mathbf{w}^{(0)}} \mathcal{L}_w^{(t)} \right)^{\top} \mathcal{H}_{\mathbf{w}^{(0)}} \left(\nabla_{\mathbf{w}^{(0)}} \mathcal{L}_w^{(t)} \right) = 0 \\
&\implies \alpha_{best}^{(t)} = \frac{\left(\nabla_{\mathbf{w}^{(0)}} \mathcal{L}_w^{(t)} \right)^{\top} \left(\nabla_{\mathbf{w}^{(0)}} \mathcal{L}_w^{(t)} \right)}{\left(\nabla_{\mathbf{w}^{(0)}} \mathcal{L}_w^{(t)} \right)^{\top} \mathcal{H}_{\mathbf{w}^{(0)}} \left(\nabla_{\mathbf{w}^{(0)}} \mathcal{L}_w^{(t)} \right)} = \frac{\left(\nabla_{\mathbf{w}} \mathcal{L}_w^{(t)} \right)^{\top} \left(\nabla_{\mathbf{w}} \mathcal{L}_w^{(t)} \right)}{\left(\nabla_{\mathbf{w}} \mathcal{L}_w^{(t)} \right)^{\top} \mathcal{H}_w \left(\nabla_{\mathbf{w}} \mathcal{L}_w^{(t)} \right)} \Big|_{\mathbf{w}^{init}}
\end{aligned} \tag{9}$$

This is the desired expression of $\alpha_{best}^{(t)}$ in Eqn. 10 in the main paper.

Note that $\mathbf{w}^{(1)}$ does not lie within the simplex. To ensure that the updated \mathbf{w} remains within the simplex, we project it onto the simplex after each gradient step. This can be done by applying the softmax operator ($\delta(\cdot)$ in the main paper), which will ensure that the updated weights are normalized and satisfy the constraints of the simplex. Moreover, in an ideal scenario, one would calculate the optimal step size $\alpha_{best}^{(t)}$ after each gradient step, taking into account the updated point. However, for the purpose of our experiment, we calculate $\alpha_{best}^{(t)}$ only for the first step and use this value as the learning rate for the remaining steps in order to avoid hessian calculation repeatedly. In our experiment, we limit the number of steps to 5 in order to ensure quicker inference. Empirically, we have observed that using the obtained step size as fixed throughout the optimization process works reasonably well.

References

Chen, L.-C.; Zhu, Y.; Papandreou, G.; Schroff, F.; and Adam, H. 2018. Encoder-decoder with atrous separable convolution for semantic image segmentation. In *Proceedings of the European conference on computer vision (ECCV)*, 801–818.

Cordts, M.; Omran, M.; Ramos, S.; Rehfeld, T.; Enzweiler, M.; Benenson, R.; Franke, U.; Roth, S.; and Schiele, B. 2016. The cityscapes dataset for semantic urban scene understanding. In *Proceedings of the IEEE conference on computer vision and pattern recognition*, 3213–3223.

Hu, X.; Fu, C.-W.; Zhu, L.; and Heng, P.-A. 2019. Depth-attentional features for single-image rain removal. In *Proceedings of the IEEE/CVF Conference on computer vision and pattern recognition*, 8022–8031.

Oymak, S.; Li, M.; and Soltanolkotabi, M. 2021. Generalization guarantees for neural architecture search with train-validation split. In *International Conference on Machine Learning*, 8291–8301. PMLR.

Sakaridis, C.; Dai, D.; Hecker, S.; and Van Gool, L. 2018. Model adaptation with synthetic and real data for semantic dense foggy scene understanding. In *Proceedings of the european conference on computer vision (ECCV)*, 687–704.

Sakaridis, C.; Dai, D.; and Van Gool, L. 2021. ACDC: The adverse conditions dataset with correspondences for semantic driving scene understanding. In *Proceedings of the IEEE/CVF International Conference on Computer Vision*, 10765–10775.